Journal of JSEM, Vol. 8, Special Issue (2008) 83-87

Digital Simulation of a Circular Ring Loaded by a Diametric Compression for Photoelastic Analysis

Yudai NOMURA[1] Pichet PINIT[2] and Eisaku UMEZAKI[1]

[1] Nippon Institute of Technology, 4-1 Gakuendai, Miyashiro, Saitama 345-8501, Japan
[2] King Mongkut's University of Technology Thonburi, 126 Prachautid, Bangmod, Thungkru, Bangkok 10140, Thailand

Abstract
New phase unwrapping algorithm is verified for its performance in unwrapping the isoclinic parameter. Both numerical and experimental photoelastic fringes of the circular ring under compression are generated for unwrapping. Comparisons between the numerical and experimental results show that the phase unwrapping algorithm is robust regardless the presence of the singularities in the isoclinic map. This shows an advance of the phase unwrapping for solving the complex fringe patterns.

Key words
Digital Photoelasticity, Digital Simulation, Circular Ring, Isotropic Point, Singular Point

1. Introduction

In (digital) photoelastic analysis, one has to determine the isoclinic parameter, ϕ, and isochromatic parameter, δ or fringe order, N. The former enables the directions of principal stresses to be evaluated whereas the latter enables the magnitude of the stress difference ($\sigma_1 - \sigma_2$) to be determined.

Most of previously published works in the field of photoelasticity do success to determine such parameters with a reasonable accuracy corresponding to their mathematical models of intensity equations associated with the types of the polariscope used. Of these methods, the circular disk model under a diametric compressive load is often used to confirm their performance. This model becomes a standard model because it has well-known mathematical formulas for determination of both parameters which in turn can be used to reconstruct theoretically photoelastic fringes. With these theoretical fringes, any developed techniques can be examined and also qualitative analysis can be done simply.

However, the circular disk model has a big limitation. That is, this model is not appropriate for fringe order numbering as the fringe field is too simple [1]. Some various aspects of a general fringe field such as source, sink, saddle point, singular point and isotropic point are not present, particularly the isotropic point, despite the fact that their existence is the main cause of failure in the determination of the isoclinic parameter which in turn affects the determination of isochromatic one. The reason is that, around these points, discontinuities in the form of sharp phase jump are present and they would fail those previously published methods, which have been tested only with the circular disk model, when these methods are applied to other models having those points.

With this problem, one should look for other models that have those aspects when they are under load to be as the new standard model or benchmark problem.

One of candidate models is a circular ring under diametric compression. The elastic solution of this model was proposed by Chianese and Erdlac [2]. By using these stress components in the Cartesian coordinates, the magnitude and directions of the principal stresses can be given. However, it is known that the formula used to determine the principal-stress directions provides the ambiguity or wrapped results even though it is theoretically derived.

This work, then, presents the comparison between the results obtained from theory and simulation. Furthermore, the results given from the simulation are unwrapped using the technique recently proposed by Pinit and Umezaki [3] such that the parameter involved presents in its physical range and, then, compared with the experiment. These comparisons are to show that the circular ring can be used as a new standard model in photoelasticity and to confirm the performance of the phase unwrapping [3].

2. Generation of Photoelastic Fringe

The computer generation of the photoelastic fringe pattern is based on the use of plane polariscope. Therefore, the expressions of the intensity I for both dark- and bright-field configurations are, respectively, [1]

$$I_\lambda = I_{p,\lambda} \sin^2(\pi N_\lambda) \sin^2 2(\phi - \theta) + I_{b,\lambda} \tag{1}$$

and

$$I_\lambda = I_{p,\lambda} [1 - \sin^2(\pi N_\lambda) \sin^2 2(\phi - \theta)] + I_{b,\lambda} \tag{2}$$

where $I_{p,\lambda}$ is the intensity coming out of the polarizer, N_λ is the relative or fractional fringe order for a given primary wavelength λ, ϕ is the isoclinic parameter or the angle between σ_1 direction and the reference axis (horizontal axis), θ is the induced phase-shifted angle and $I_{b,\lambda}$ is the background intensity. These two equations play a major role in determination of photoelatic parameters.

2.1 Conditions for fringe generation

For fringe generation according to Eq. (1) or (2), the following two conditions are assumed, i.e.,

- $I_{p,\lambda}$ is set to be equal to the maximum gray level value of the hardware used. In this work, 256-shaded gray level is used; thus, $I_{p,\lambda} = 255$.

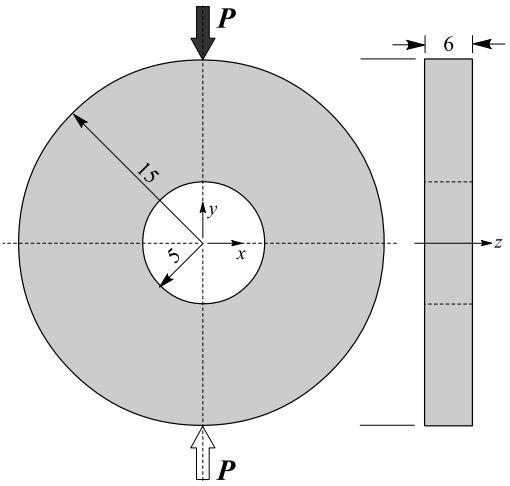

Fig. 1. Geometrical shape of the circular ring and the applied compressive load (P = 274 N) exerted along the vertical diametral line. The black and white arrows show the points of applied load and of reaction, respectively. (Geometrical unit: mm, image not to scale.)

- $I_{b,\lambda} = 0$. Since $I_{p,\lambda}$ is only the dc or constant term of the signal, its effect is only to force the intensity profile upwards. Then, it can be of any value as long as the value of intensity I_λ does not exceed $I_{p,\lambda}$. In this work, for simplicity, it is set as shown.

2.2 Acquisition of N and ϕ

For fringe order N_λ, it can be obtained from the well known relation [1]

$$\left(\frac{N_\lambda f_{\sigma,\lambda}}{2}\right)^2 = (\sigma_{xx} - \sigma_{yy})^2 + \tau_{xy}^2 \tag{3}$$

where $f_{\sigma,\lambda}$ is the material stress fringe value obtained from calibration. The Cartesian stress components σ_{xx}, σ_{yy} and τ_{xy} can be given from reference [2]. The angle ϕ is theoretically expressed as the following relation [4]

$$\tan 2\phi_{\angle\sigma_1,\sigma_2} = \frac{2\tau_{xy}}{\sigma_{xx} - \sigma_{yy}} \tag{4}$$

The subscript $\angle\sigma_1,\sigma_2$ denotes that ϕ map can refer to either σ_1 or σ_2 direction. It is informative to note that even though Eq. (4) is theoretically derived, ambiguity for which the computed ϕ value represents the direction of σ_1 or σ_2 still exists. Equation (4) can also be found on many standard text books of Strength of Materials but descriptions relating to the formation of singularities caused by the stress components in Eq. (4) can be found in reference [4].

3. Computation of Isoclinic Parameter

The equation for numerically determining the isoclinic parameter ϕ using the computer generated photoelastic fringe patterns obtained on the basis of four-step color phase shifting technique is expressed as [3,5]

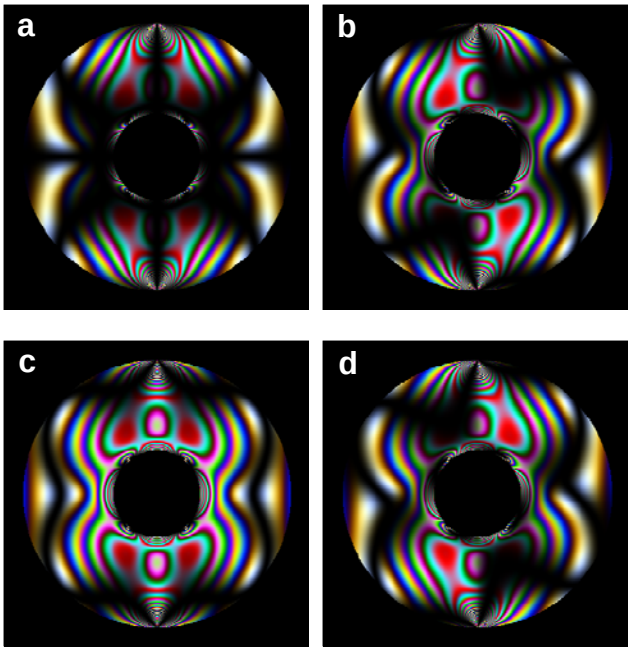

Fig. 2. Computer generated color photoelastic fringe pattern obtained using Eqs. (1), (3) and (4) using the Cartesian stress components σ_{xx}, σ_{yy} and τ_{xy} obtained from the analytic solution. (a) fringe pattern of $I_{1,\lambda}$ (θ = 0), (b) fringe pattern of $I_{2,\lambda}$ (θ = π/8), (c) fringe pattern of $I_{3,\lambda}$ (θ = π/4), and (d) fringe pattern of $I_{4,\lambda}$ (θ = 3π /8).

$$\phi_{\angle\sigma_1,\sigma_2} = \frac{\pi}{8} - \frac{1}{4}\arctan\left(\frac{I_1^s - I_3^s}{I_2^s - I_4^s}\right) \tag{5}$$

Equation (5) mathematically gives $\phi_{\angle\sigma_1,\sigma_2} \in [0, +\pi/4]$ due to the use of the (ordinary) arctangent function and this wrapped phase range is termed as the base-wrapped phase range [3]. Note that $(a, b]$ represents $a < x \le b$ in which x is a variable of interest. Furthermore,

$$I_m^s = \sum_{\lambda=R,G,B} I_{m,\lambda} \quad \text{for } m = 1,2,3,4 \tag{6}$$

and

$$I_{mod}^s = \sum_{\lambda=R,G,B} I_{p,\lambda} \sin^2(\pi N_\lambda) = \sqrt{(I_1^s - I_3^s)^2 + (I_2^s - I_4^s)^2} \tag{7}$$

Detail about the normalization of values given from Eq. (6) before substituting into Eq. (5) can be found in references [3,5]. Note that in mathematical sense, Eq. (5) is valid only if $I_{mod}^s \neq 0$. However, for the experimental data, this is not true. Equation (5) is invalid when $I_{mod}^s = 0$.

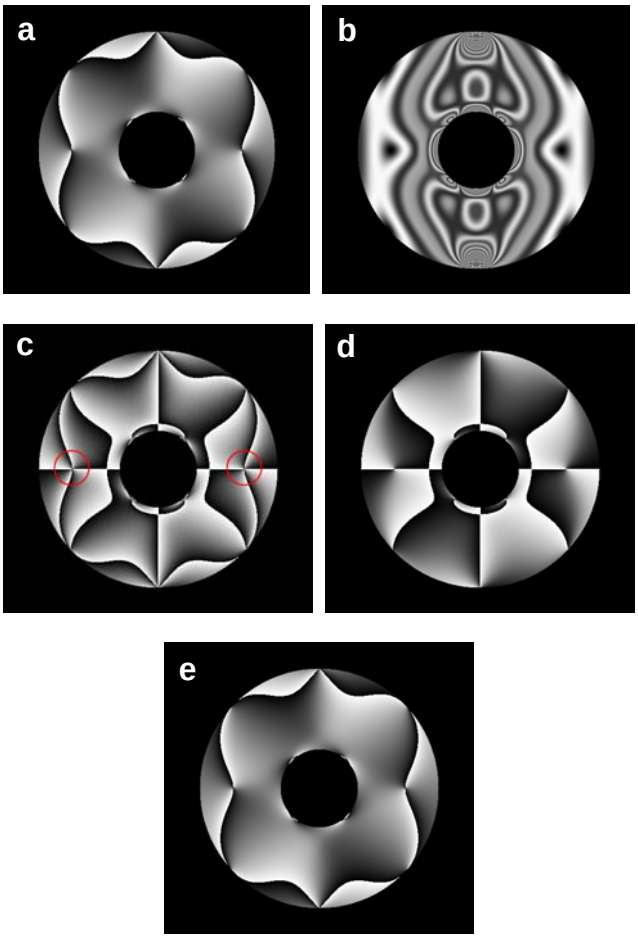

Fig. 3. Results obtained from theory and simulation. (a) theoretical map of wrapped isoclinic computed using Eq. (4), $\phi_{\angle\sigma_1,\sigma_2} \in (-\pi/4, +\pi/4]$, (b) modulation intensity map obtained from I^s_{mod} expressed in Eq. (7) associated with the number of wavelengths used (λ = R, G, B, (c) map of $\phi_{\angle\sigma_1,\sigma_2} \in [0, +\pi/4]$ given from Eq. (5), (d) map of $\phi_{\angle\sigma_1,\sigma_2} \in [0, +\pi/2]$, and (e) map of $\phi_{\angle\sigma_1,\sigma_2} \in (-\pi/4, +\pi/4]$. (d) and (e) were obtained from (c) using the simple logic operations (comparison of intensity). Note that their values are separately and linearly mapped into 256-shaded gray levels by which 0 represents deep black and 255 represents pure white. Red circles in (c) show the position of the isotropic points.

For some specific values of I^s_{mod}, its effect on the map of isoclinics is clearly seen. Further, the modulation intensity obtained from Eq. (7) is used in the isotropic point detection algorithm [3].

4. Results and Discussion

Figure 1 shows the geometrical shape of the circular ring model used for computer generation of photoelastic fringe patterns. The material fringe values used in the fringe simulation code were obtained from the calibration of a bending beam made of an epoxy resin plate at three wavelengths; that is, $\lambda_R = 612$, $\lambda_G = 547$, and $\lambda_B = 437$ nm.

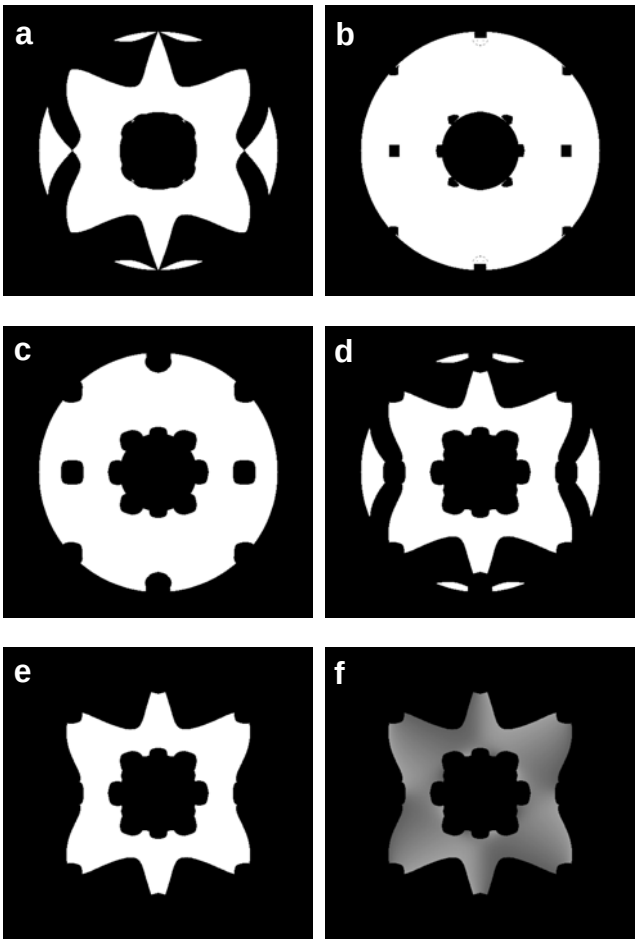

Fig. 4. Necessary binary images for the phase unwrapping technique proposed in reference and the first valid region of correct values of isoclinic angle. (a) valid region, (b) regions representing the positions of the isotropic points (complete blocks) and singular points (uncompleted blocks), (c) expand regions of isotropic points and singular points in (b), (d) result of intersection of (a) and (c), (e) result obtained from the application of the connected component labeling to (d), and (f) first valid region of correct values of isoclinic angle obtained by overlaying (e) over Fig. 3e.

The material stress fringe values are, then, $f_{\sigma,R} = 11.20$, $f_{\sigma,G} = 10.01$, and $f_{\sigma,B} = 8.000$ N/(mm·fringe).

4.1 Computer generated photoelastic fringe

After obtaining N and ϕ from Eqs. (3) and (4) using the Cartesian stress components given by the analytical solution [2], they are, then, substituted into Eq. (1) and the photoelastic fringe patterns are given based on the four-step phase shifting technique with discrete wavelengths of plane-polarized RGB light [5, 6].

Figure 2 shows the computer generated photoelastic fringe. Nevertheless, from these fringe patterns, it is very difficult to identify the position of the singular point(s) and isotropic point(s).

Fig. 5. Numerical map of unwrapped isoclinics in the range (−π/2, +π/2] computationally obtained from the phase unwrapping technique [3].

4.2 Theoretical and numerical results of ϕ

Figure 3a shows the map of wrapped isoclinics in the range (−π/4, +π/4] obtained using Eq. (4). Figure 3b displays the map of modulation intensity of I^{s}_{mod} obtained using Eq. (7). This modulation intensity map is necessary in the isotropic point detection [3].

Figure 3c shows the maps of wrapped isoclinics in the range $\phi_{\angle\sigma_1,\sigma_2} \in [0, +\pi/4]$ computed using Eq. (5) whereas Figs. 3d and e report the map of wrapped isoclinics $\phi_{\angle\sigma_1,\sigma_2} \in [0, +\pi/2]$ and $\phi_{\angle\sigma_1,\sigma_2} \in (-\pi/4, +\pi/4]$, respectively. They were given from Fig. 3c based on the intensity comparison [3]. Note that Fig. 3b can be used for evaluation of N because the fringe pattern is of the intensity data that is solely the function of N.

It is seen that the map of wrapped isoclinics shown in Figs. 3a and e are identical. This certifies that the numerical result agrees well with that of theory. The position of the isotropic points can be clearly seen in Fig. 3c (red circles). However, one can see the isotropic points in all maps.

Due to the mechanical stability of the isotropic points, their positions appear in all maps of isoclinics (compare the positions of the isotropic points in Figs. 3c, d and e). Further, it is seen that the positions of the isotropic points are obviously observed in Fig. 3b. This is because the fringe order values of N are equal to zero there (zero fringe order). However, it is quite difficult for a non-expert or non-photoelastician to recognize them because the zero order fringe and the first order fringe gray shades resemble.

Figures 4a-e show all the binary images needed for the phase unwrapping technique proposed in reference [3] whereas Fig. 4f shows the first region of the correct isoclinic angle values. Figure 4a is the valid region identified by a half of $\phi_{\angle\sigma_1,\sigma_2} \in (-\pi/4, +\pi/4]$; that is, the white pixels in the image refer to $\phi_{\angle\sigma_1,\sigma_2} \in (-\pi/8, +\pi/8]$.

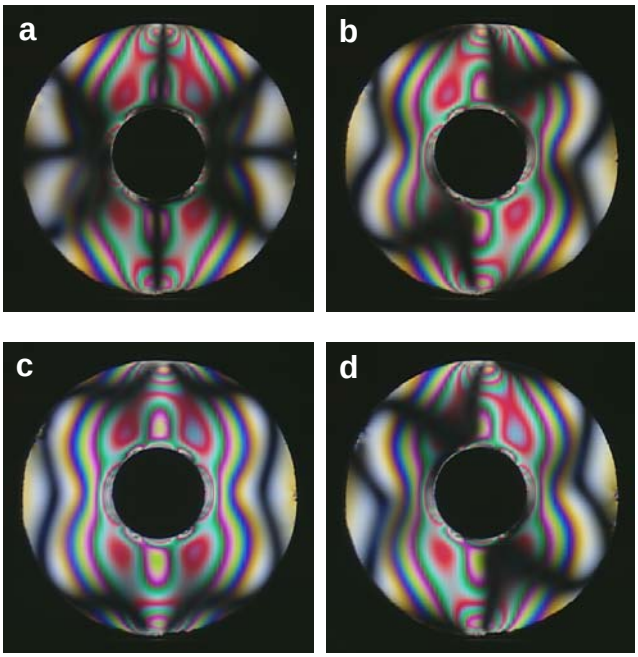

Fig. 6. Experimentally generated color photoelastic fringe pattern obtained using the dark-field configuration of plane polariscope with the tricolor light source. (a) fringe pattern of $I_{1,\lambda}$ (θ = 0), (b) fringe pattern of $I_{2,\lambda}$ (θ = π/8), (c) fringe pattern of $I_{3,\lambda}$ (θ = π/4), and (d) fringe pattern of $I_{4,\lambda}$ (θ = 3π/8).

The positions of the isotropic and singular points were found by the detection algorithm and they are shown in Fig. 4b whereas Fig. 4c shows their expansion. The window size for detecting and expanding were of 21 × 21 pixels.

Figure 4d was obtained by the intersection operation between Figs. 4a and c. The positions of the isotropic points, singular points and poles (load application points) were discarded from Fig. 4a. Applying the connected component labeling algorithm to Fig. 4d yields binary image shown in Fig. 4e. Then, the first region of the correct isoclinic-angle values is shown in Fig. 4f. This region was obtained by selecting the isoclinic-angle values from Fig. 3e using Fig. 4e as a filter.

Figure 5 shows the map of unwrapped isoclinics in the range (−π/2, +π/2] with modulo π obtained from using the algorithm described in Reference [3]. The brief procedures are as follows. All pixels at the boundary of Fig. 4f are detected and kept to be a starting pixel by the help of Fig. 4e. These pixels are used as a central pixel of a 3 × 3 unwrapping window. To-be-unwrapped pixels in this window are unwrapped comparing to the central pixel. The final value of the wrapped pixel is determined on the basis of the comparison of the pixel values of maps shown Figs. 3d and e with certain conditions [3].

As seen in this map (Fig. 5), the positions of all isotropic points and singular points can be seen. It is to be note that the isotropic points in this model are of positive type [4].

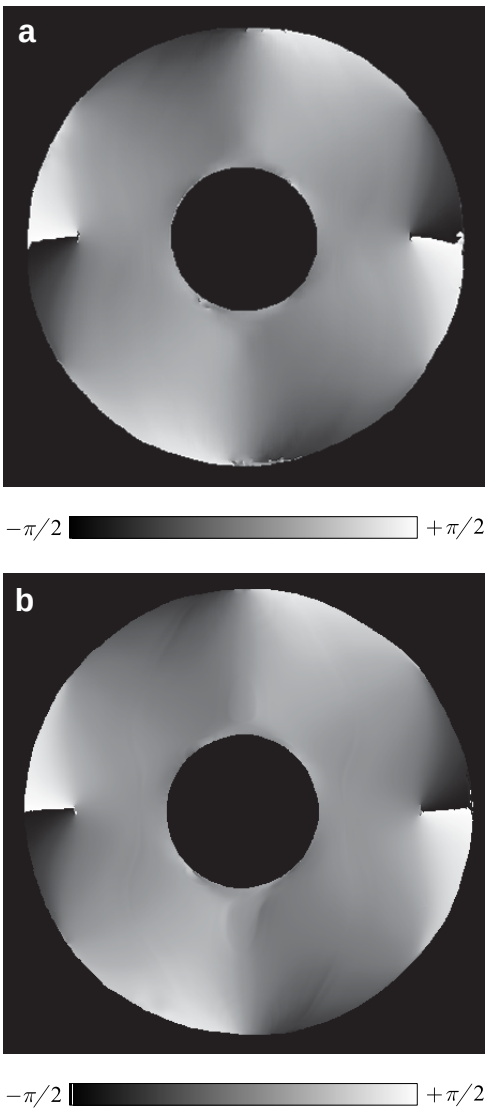

Fig. 7. Maps of unwrapped isoclinics in the range (−π/2, +π/2]. (a) map obtained from the use of those experimentally photoelastic fringe patterns generated with the tricolor light source as shown in Fig. 6 and (b) map obtained from the use of those experimentally generated photoelastic fringe patterns generated with the white light source (images not shown here).

4.3 Experimental results of ϕ

Figure 6 shows the experimentally generated fringe patterns captured from the dark-field configuration of plane polariscope with a tricolor light source [5, 6]. Comparing Fig. 2 to Fig. 6 reveals that photoelastic fringe patterns are nearly similar.

Figure 7a shows the map of unwrapped isoclinics in the range (−π/2, +π/2] with modulo π obtained using the fringe images shown in Fig. 6 whereas Fig. 7b was the map of unwrapped isoclinics given from the use of the photoelastic fringe images digitally recorded with the white light source [3]. These fringe images are, however, not shown here. It is easily seen in Fig. 7 that all isoclinics passing through the isotropic points gradually vary from −π/2 to +π/2 counterclockwise around such points. Hence, the isotropic points are of positive type [4].

Qualitative comparison of Fig. 7 and Fig. 5 reveals that they are almost alike; however, the difference can be seen in Fig. 7a where the end of period occurs (the locations at which the isoclinics rapidly change from −π/2 to +π/2). This difference actually was not the result of the phase unwrapping technique but, instead, it is the result of the imperfection of the photoelastic model and the experiment done at different time.

Singular points locating on the inner boundary are clearly observed whereas those points lying on the outer boundary are rather vague (Fig. 5). However, for the maps shown in Fig. 7, such points cannot be seen. The imperfection of the model might cause this. In addition, one can see the unsmooth area of the isoclinics near the lower inner boundary. This area becomes clearly seen because of the effect of the isochromatic parameter since Fig. 7b was given from images captured using white light.

5. Conclusion

The phase unwrapping technique recently proposed by the present authors has been verified for its performance in the unwrapping of isoclinic parameter. The results of the maps of unwrapped isoclinics numerically and experimentally obtained from three different sets of the photoelastic fringe patterns show good agreement.

Generally, in photoelasticity, the circular disk under compressive load is used as the standard model for verification the performance of any developed method since it has theoretical formula for the reconstruction of the isochromatic parameter. However, this model lacks the important features as previously mentioned.

It has been shown that the results obtained from the phase unwrapping developed by the authors provides the results of both circular disk and circular ring [3] and the correctness of the results of the circular ring is confirmed here. Therefore, the circular ring can be leveled up to be the new standard model in photoelasticity.

References

[1] Ramesh, K.: *Digital Photoelasticity: advanced techniques and applications*, Springer, Berlin (2000), 157, 231.

[2] Chinese, R.B. and Erdlac, R.J.: *Q. Jl Mech. appl. Math.*, **41** (1988), 239-247.

[3] Pinit, P. and Umezaki, E.: *Opt. Lasers Eng.*, **45** (2007), 795-807.

[4] Frocht, M.M.: *Photoelasticity*, Vol. 1, John Wiley & Sons, New York (1941), 12, 189-190, 194-195.

[5] Pinit, P. and Umezaki, E.: *Opt. Rev.*, **12** (2005), 228-232.

[6] Pinit, P. and Umezaki, E.: *Key Eng. Material*, **326-328** (2006), 75-78.